HHS Public Access

Author manuscript

Bone. Author manuscript; available in PMC 2020 June 01.

Published in final edited form as:

Bone. 2019 June ; 123: 234–245. doi:10.1016/j.bone.2019.03.031.

Vasculature Submucosal Changes at Early Stages of Osteonecrosis of the Jaw (ONJ)

Ioannis Gkouveris[1], **Danny Hadaya**[1], **Akrivoula Soundia**[1], **Olga Bezouglaia**[1], **Yee Chau**[1], **Sarah Dry**[2], **Flavia Q Pirih**[3], **Tara L Aghaloo**[1,*], **Sotirios Tetradis**[1,*]

[1)]Division of Diagnostic and Surgical Sciences, UCLA School of Dentistry, Los Angeles, CA 90095, USA.

[2)]Department of Pathology and Laboratory Medicine, David Geffen School of Medicine at UCLA, Los Angeles, CA 90095, USA.

[3)]Division of Constitutive and Regenerative Sciences, UCLA School of Dentistry, Los Angeles, CA, 90095, USA

Abstract

Osteonecrosis of the Jaw (ONJ), a rare, but potentially severe side effect of anti-resorptive medications, presents as exposed bone in the maxillofacial region lasting for at least 8 weeks. While clinical experience and animal models concur in finding that systemic antiresorptive treatment in conjunction with local risk factors, such as tooth extraction or dental disease may lead to ONJ development, the subclinical molecular changes that precede bone exposure remain poorly understood. The identification of these changes is not only important in understanding disease pathophysiology, but could provide potential for treatment development. Here, we evaluated the early stages of ONJ utilizing a model of experimental periodontitis (EP) in mice treated with two different types of antiresorptives, targeting potential changes in vasculature, hypoxia, oxidative stress, and apoptosis. Antiresorptive treatment in animals with EP increased levels of empty osteocytic lacunae and increased ONJ prevalence compared to Veh animals. The arteriole and venule network seen around EP areas was diminished in animals treated with antiresorptives. Higher levels of vascular endothelial growth factor A (VEGF -A) and vascular cell adhesion protein-1 (VCAM-1) were observed 1-week following EP in treated animals. Finally, levels of hypoxia, oxidative stress, and apoptosis remained high in antiresorptive treated animals with EP through the duration of the experiment. Together, our data point to subclinical vasculature organizational disturbances that subsequently affect levels of hypoxia, oxidative stress, and apoptosis in the area of developing ONJ.

1. INTRODUCTION

Osteonecrosis of the jaws (ONJ), a potentially severe side effect of anti-resorptive and anti-angiogenic medications, presents as exposed bone in the maxillofacial region that lasts for

*Corresponding Authors: Sotirios Tetradis DDS, PhD, UCLA School of Dentistry, 10833 Le Conte Ave. CHS Rm. 53-068, Los Angeles, CA 90095-1668, Tel: (310) 825-5712, Fax: (310) 825-7232, stetradis@dentistry.ucla.edu; Tara L. Aghaloo DDS, MD, PhD, UCLA School of Dentistry, 10833 Le Conte Ave. CHS Rm. 53-009, Los Angeles, CA 90095-1668, Tel: (310) 794-7070, Fax: (310) 825-7232, taghaloo@dentistry.ucla.edu.

more than eight weeks, in the absence of head and neck radiation therapy [1, 2]. Antiresorptive agents, such as bisphosphonates (BPs) and denosumab (Dmab) are commonly used for the management of osteoporosis, multiple myeloma, bone metastasis, and other bone diseases characterized by excessive bone resorption [3, 4]. Although initially described in 2003, ONJ pathophysiology has not been fully delineated; several hypotheses implicate suppression of bone resorption, trauma, immune dysfunction, infection/inflammation or blood supply inhibition [5]. However, the extent of involvement for each factor remains controversial and none are adequate to explain the full spectrum of ONJ presentation. While these controversies remain, it is now well-accepted that systemic antiresorptive therapy combined with local dental risk factors, such as tooth extraction, can lead to ONJ development [6].

Interestingly, ONJ presentation in patients treated with both BPs and Dmab is similar in appearance with comparable prevalence rates [1, 7], despite the distinct molecular mechanisms of action of BPs and Dmab. Thus, inhibition of osteoclastic function appears to play a central role in ONJ pathogenesis. Nevertheless, how inhibition of bone resorption leads to defective soft tissue and osseous healing and results in clinical bone exposure remains unclear [8]. Dental or gingival/periodontal disease increase ONJ risk, while infection and trauma are also reported as causes for disease initiation [9].

As a result, several reports focus on the role of soft tissue in disease pathophysiology. Indeed, chronic alendronate therapy affects terminal differentiation, proliferation and epithelial adhesion of epithelial cells in clinically healthy human oral mucosa [10]. Similarly, BP treatment induces apoptosis of human periodontal fibroblasts and keratinocyte cell lines with enhanced expression of apoptotic markers [11, 12]. While in-vitro studies may provide insight on pathogenesis, these cells are removed from their natural environment, and thus do not mimic physiologic disease states. However, observations have also been made in the oral mucosa of patients with ONJ lesions. The reduction of vascular endothelial growth factor type A and angiogenin-1, known regulators of angiogenesis, is a common observation in patients with ONJ. [13, 14]. In the osseous environment, BPs suppress angiogenesis following tooth extraction [15]. In addition, microvasculature defects have been described at the margins of well-established ONJ lesions [16]. Nevertheless, it is not clear if these changes are the result or the cause of ONJ development.

The sequence of subclinical events and changes that lead to clinical bone exposure is poorly understood, and has yet to be investigated. While previous studies provide significant insight on disease pathophysiology, they are observed after established ONJ occurs. Importantly, no causative association can be made, nor can chronologic changes be assessed. Here, we hypothesize that vascular changes in the mucosal and osseous environment precede the development of ONJ in association with antiresorptive treatment.

Our previous studies have shown that combined periodontal or periapical disease and antiresorptives are sufficient to induce ONJ-like lesions in the absence of tooth extraction [17, 18]. Taking advantage of this established ONJ animal model, now we studied early vascular changes in the submucosa around areas of developing ONJ.

2. MATERIALS AND METHODS

2.1 Animal Care

This experimental protocol was approved by the UCLA institutional animal care and use committee (IACUC). Animals were kept and treated according to IACUC guidelines. Throughout the experimental period, mice were housed in plastic cages, fed a soft diet (Bacon Softies, BioServe, Flemington, NJ, USA), and given water ad libitum. One hundred-eight 2-month old C57BL/6J male mice (Jackson Laboratories, Bar Harbor, ME, USA) were randomly assigned, by bodyweight, to receive intraperitoneal (IP) injections of Veh (endotoxin free saline), 200 μg/kg zoledronic acid (ZA, Z-5744 LKT Laboratories, St. Paul, MN, USA) twice a week, or 10 mg/kg OPG-Fc (Amgen, Inc, Thousand Oaks, CA, USA) twice per week. OPG-Fc, an inhibitor of the receptor activator of N F -κB ligand (RANKL), mimics Dmab function in rodents, and has been effectively and extensively used in animal studies at this dose [19].

Mice were pre-treated with Veh, ZA, or OPG-Fc for a week. Then, 6–0 silk ligatures were placed around the right maxillary second molar of all animals to induce Experimental Periodontitis (EP) of the right maxilla. No ligature was placed around the left maxillary molarsof any mouse, enabling all left maxillary second molars to establish the left maxillary periodontium as a non-EP control. Twelve mice per treatment group (12 Veh, 12 ZA, 12 OPG-Fc for a total of 36 mice per time-point) were sacrificed at the first, second and fourth week following ligation. Treatment continued through the duration of the experiment. Animals were euthanized via isoflurane overdose, and maxillae containing the right maxillary molars with EP and the left maxillary molars without EP were dissected, placed in 4% paraformaldehyde for 48 hours and stored in 70% ethanol.

2.2 μCT scanning

Dissected maxillae were imaged by specimen μ,CT (11μm) utilizing the SkyScan 1172 μCT scanner (SkyScan, Kontich, Belgium), as described [20, 21]. Volumetric data were converted to DICOM format and imported in the Dolphin Imaging (Chatsworth, CA, USA) software to generate 3D images. Multiplanar reconstructed images were obtained, where measures were made in the sagittal and coronal cross sections. Alveolar bone height (ABH) was assessed by measuring the distance from the alveolar crest to the Cemento-Enamel Junction (CEJ) at the mesial and distal aspect of the second molar, as described [17, 21]. All scans were de-identified and evaluated in random order with investigators being blinded to treatment.

2.3 Histology

Tissues from all time-points were processed simultaneously. Maxillae were decalcified in 14% EDTA for 3 weeks. Samples were paraffin embedded and 5 μm-thick cross sections were at the coronal plane, perpendicular to the mid-palatal suture. Each sample was trimmed to a standardized location, defined by the presence of the mesial and palatal roots. The first section was stained with hematoxylin and eosin (H&E), and subsequent sections were used for immunofluorescence staining, described below. H&E stained slides were digitally scanned utilizing the Aperio AT automated slide scanner and automated image analysis was performed using the Aperio Image Scope software (Aperio Technologies, Inc., Vista, CA,

USA). The area of the alveolar bone, from the alveolar crest to the floor of the nasal cavity was defined as the region of interest (ROI). The total number of osteocytic lacunae and the number of empty lacunae were quantified. The number of lacunae evaluated ranged from 100–250. Osteocytes that appeared to have undergone pyknosis, karyorrhexis, or karyolysis, and those with eosinophilic cytoplasm [22] were counted as empty lacunae. The shortest distance from the inferior part of the epithelium to the most coronal point of the alveolar crest was measured on both buccal and palatal sides of the maxilla and was averaged for each mouse. For prevalence assessment, ONJ was defined as exposed bone, in conjunction with the clinical definition by the American Association of Oral and Maxillofacial Surgeons (AAOMS) [2]. All histology and digital imaging was performed at the Translational Pathology Core Laboratory (TPCL) at the David Geffen School of Medicine at UCLA.

2.4 Immunofluorescence staining analysis

Immunofluorescence staining of tissue sections were probed with rabbit polyclonal antibodies against α-SMA(ab5694, Abcam, 1:200), 4-HNE (ab46545, Abcam, 1:200), cleaved caspase-3 (#9661, Cell Signaling, CA, USA, 1:250), rabbit monoclonal antibody against VEGFA (ab52917, Abcam, 1:200), rat monoclonal antibody against VCAM-1 (FITC-conjugated, ab24853, Abcam, 1:200), mouse monoclonal HIF-1α antibody (Alexa Fluor® 488-conjugated, sc-13515, Santa Cruz Biotechnology, USA, 1:250) and goat-polyclonal Endomucin antibody (Santa Cruz Biotechnology, USA, 1:250). α-SMA is an element of the contractile apparatus in smooth muscle cells, highly expressed in arteries [23], while expression of the sialoglycoprotein endomucin is localized to venules and capillaries [24].

After incubation with primary antibody overnight and three washes with PBS/T, the slides were incubated with the appropriate secondary antibody (AlexaFluor 488 donkey anti-goat or AlexaFluor 568 goat anti-rabbit, Invitrogen) at room temperature for 1 h. After three washes with PBS/T, slides were mounted using UltraCruz® Mounting Medium with DAPI staining to detect nuclei (Santa Cruz Biotechnology, Santa Cruz, CA, USA, sc-24941). As a negative control to ensure specificity of staining, the omission of the primary antibodies from the staining procedure was carried out on some samples. Photomicrographs were obtained using a fluorescence optical microscopy (Mantra, PerkinElmer, USA).

Standardized computer-assisted immunofluorescence quantification was performed using Image J (NIH). The total area was defined as the area from the ridge of the alveolar crest to the basal membrane of keratinized epithelium under the ligature and was measured manually. For total venule and arterial area, the area of each vessel was measured manually using Image J. For assessment of vessels, positively stained tubular (either α-SMA or EMCN) formations were selected. The total area was then summed. For the remaining molecules, the region of interest was selected, a minimal and maximal threshold were set and total expression was calculated. The autofluorescence of erythrocytes was manually removed from all quantification. The threshold for positive expression was adjusted for each antibody and was kept the same for all samples in all groups. All investigators performing measurements were blinded to the treatment groups and time-points.

2.5 Statistics

Raw data were analyzed using the GraphPad Prism Software (GraphPad Software, Inc. La Jolla, CA). Descriptive statistics were used to calculate the mean and the standard error of the mean (SEM). Statistical differences among Veh, OPG-Fc, and ZA groups at each time point were analyzed using a one-way ANOVA with Tukey's post-hoc test. Comparison of the three time points within each treatment group was performed using a one-way ANOVA with Tukey's post-hoc test. A Fisher exact test was used for categorical data.

3. RESULTS

The average initial body weight of all 108 mice was 19.1g ± 2.3 (mean ± SD). The average body weight for all mice necropsied at the 1w, 2w, and 4w time points were 20.5g ± 1.7, 22.3g ± 2.4, and 25.4g ± 2.8, respectively. A statistically significant increase in bodyweight was noted between the initial body weight and 4w time point. However, no differences in weight were observed among Veh, ZA, or OPG-Fc groups at any time point. For all measurements reported below, the periodontium around the left maxillary molars, without EP, were used as controls. No differences in any of the measurements for the left maxillary periodontium were noted among the Veh, ZA, or OPG-Fc groups; additionally, no changes were observed in any measurement through the duration of the experiment (Sup. Fig. 1).

3.1 Clinical, μCT and histologic assessment

Clinical photomicrographs showed the presence of the ligature around M2 in all groups. (Fig. 1B). μCT examination was conducted at the one, two, and four-week necropsy time points to investigate the effects of EP in Veh, ZA and OPG-Fc treated molars (Four-week time point is shown on Fig. 1C). In the periodontium around Veh treated EP molars, the CEJ-Alveolar Crest Distance was significantly increased compared to both ZA and OPG-Fc treated EP molars. This was observed at all time points (Fig. 1D). ABH increased significantly in the Veh treated EP periodontium from 1–4 weeks of treatment, while it remained unchanged in the OPG-Fc and ZA treated EP periodontium (Fig. 1D).

In the ligated areas of Veh treated animals, abundant inflammatory infiltrate and bone resorption were noted (Fig. 1E). In the ZA and OPG-Fc treated groups, the alveolar crest retained its height, while extensive inflammatory infiltrate was noted in close proximity to the alveolar bone (Fig. 1E). In both ZA and OPG-Fc treated EP sites, the epithelium-alveolar crest distance was decreased significantly, compared to the Veh group (Fig. 1F). Importantly, a statistically significant increase in the percent of empty osteocytic lacunae around the ZA and OPG-Fc treated EP molars was observed (Fig. 1G). The total number of osteocytic lacunae decreased in the Veh, compared to the ZA or OPG-Fc groups (Sup. Fig. 1). Interestingly, the empty osteocytic lacunae were mostly visible in the coronal portion of the alveolar bone adjacent to the ligature in the OPG-Fc and ZA groups. In the Veh animals, the empty lacunae were sparse, distributed through the coronal and apical regions of the alveolar bone. No empty lacunae were seen in non-EP tissues. A progressive increase in ONJ prevalence was observed in OPG-Fc or ZA treated animals with EP that was maximal by 4 weeks of treatment (Fig. 1H).

3.2 Immunofluorescence analysis of vasculature changes

Investigation of alterations in the vasculature network revealed that in the ZA and OPG-Fc EP groups, a statistically significant decrease in total arterial area was observed at the 1-week, 2-week, and 4-week time points. (Fig. 2A–A2, B–B2, C–C2, D). Quantification of EMCN IF staining revealed that the total venus area was similar in all treatment groups at 1 and 2 weeks; however, at the 4-week time point, the total venous area in the OPG-Fc or ZA groups was significantly less then Veh treated group of the same time point of the OPG-Fc or ZA groups of earlier time points (Fig. 3A–2, B–B2, C–C2, D).

To dissect the changes in EMCN and α-SMA, IF analysis of VEGF-A (Fig. 4), a growth factor with pivotal role in angiogenesis, and VCAM-1 (Fig. 5), a cellular adhesion molecule, was conducted. Quantification of VEGF-A revealed an increase in VEGF in all treatment groups at 1-week of treatment, compared to non-EP sites (Fig. 4G). At the 1-week time point, a statistically significant increase was noted in the ZA and OPG-Fc treated EP alveolar tissue, in comparison to Veh (Fig. 4A–A1, B–B1, C–C1). By 4-weeks of treatment, levels in Veh treated EP sites remained similar to the 1 week timepoint; in comparison, ZA and OPG-Fc EP sites declined significantly, compared to their 1-week and 2-week levels (Fig. 4D–D1, E–E1, F–F1, G). Additionally, at the 4 week timepoint, the OPG-Fc and ZA groups were significantly lower than Veh group (Fig. 4G). A similar trend was observed in the IF evaluation of VCAM-1. At 1-week following EP, IF levels of VCAM-1 were increased in all treatment groups, compared to non-EP. A statistically significant increase in OPG-Fc and ZA EP alveolar tissue was noted compared to Veh EP sites(Fig. 5A–A1, B–B1, C–C1, G). At 4-weeks of treatment, VCAM-1 levels in veh animals did not change; however, in the ZA or OPG-Fc treated groups, VCAM-1 esxpression decreased significantly compared to the Veh group at 4-weeks of treatment, or to the 1 and 2-week time points (Fig. 5D–D1, E-E1, FF1, G).

3.3 Immunofluorescence analysis of oxidative stress, hypoxia, and apoptosis

HIF-1α, a regulator of cellular responses to hypoxia, and 4HNE, a marker of oxidative stress, were assessed using IF (Fig. 6 and 7, respectively). HIF-1α expression was increased in all groups compared to healthy, non-EP alveolar tissue. A statistically significant increase in HIF-1α expression was seen in the ZA and OPG-Fc group, compared to the Veh group, at 1 week of treatment (Fig. 6D). This trend, with high levels of HIF-1α at ZA and OPG-Fc, continued through the duration of the experiment (Fig. 6D). A similar trend was seen in the marker, 4HNE, with generally increased levels compared to healthy, non-EP values in all groups (Fig. 7D). Again, a statistically significant increase was seen in the sites around ZA and OPG-Fc ligated molars at 1-week, when compared tissue around Veh ligated molars, which continued through the experiment (Fig. 7D).

Cleaved Caspase-3, a marker of apoptosis, increased in all treatment groups with EP, when compared to non-EP (Fig. 8D). However, a significant increase was observed in the alveolar tissue ZA and OPG-Fc molars with EP, when compared to sites around Veh molars with EP, at 1-week. By 4-weeks of treatment, cleaned caspase-3 had increased, and reached peak levels in ZA and OPG-Fc treated groups, while remaining steady in the Veh group (Fig. 8D).

4. DISCUSSION

ONJ is a significant complication of antiresorptive medications that are used to treat bone diseases characterized by excessive bone resorption. Since its initial appearance in literature, significant strides have been made in disease understanding. Systemic and local risk factors known to exacerbate ONJ development have been identified [1, 25, 26]. Indeed, tooth extraction is the most common instigating factor in ONJ development in humans taking anti-resorptives [1, 27]. Animal models have used tooth extraction to capture several of the characteristics of ONJ in various experimental settings [15, 28–30]. In addition to tooth extraction, we and others, have used experimental periodontal or periapical disease as a local instigating factor for ONJ development [17, 18, 31].

These animal models, combined with clinical observations, point to the pathogenic role of dental disease in ONJ pathophysiology. Not utilizing tooth extraction, avoids disruption of soft tissue integrity that complicates the environment of mucosal and osseous healing, thus allowing the investigation of subclinical events in the process of ONJ development. With this in mind, here, we used an established animal model of experimental periodontitis (EP) in combination with high dose antiresorptives to study early cellular and molecular responses of periodontal tissues in control vs. treated animals. We utilized the bisphosphonate ZA and the RANKL inhibitor OPG-Fc, as two different classes of antiresorptives with distinct molecular mechanisms, to detect changes due to inhibition of resorption rather than a specific response to either of the two agents.

To confirm the presence of developing ONJ, we performed histologic analysis to evaluate the presence of empty osteocytic lacunae. In the absence of EP, ABH remained similar in Veh, OPG-Fc, and ZA groups. In addition, the absence of inflammatory infiltrate or empty osteocytic lacunae in all groups was observed (data not shown). In the Veh group with EP, an inflammatory infiltrate was observed around the ligated area with a loss of ABH with very few empty osteocytic lacunae and fewer total lacunae than in OPG-Fc and ZA groups. This is in strong contrast to the OPG-Fc and ZA treated animals, where empty osteocytic lacunae were observed in the coronal portions of the retained alveolar bone. These findings indicate that antiresorptives did not cause diffuse osteonecrosis throughout the alveolar bone, but raises the possibility that inflammation or infection caused necrosis of bone tissue that could then not be resorbed due to action of the anti-resorptive agent. This confirms our previous findings, where necrotic areas were localized at the alveolar crest in mice with experimental periapical disease [18].

We then explored changes in the vasculature network by identifying arteries (α-SMA) and veins (EMCN) around areas of EP. Indeed, as early as one week following disease initiation and extending for the duration of the experiment, a significant decrease in total arterial area in both ZA and OPG-Fc treated animals was observed. This decrease in arterial area was accompanied by a decrease in total venous area that became apparent by 4 weeks of treatment. These observations show a vascular disparity in the EP sites with an overall decrease in vascularity during antiresorptive treatment. Interestingly, similar observations have been made in patients with ONJ, where narrow, hypo-vascularized spaces are observed around mucosal margins of ONJ lesions [16]. The fact that these patient findings are

observed in established ONJ lesions, while our studies were done at early time points suggests that vascular changes could be a constant feature of ONJ lesions from the initial stages to the final clinical presentation.

Following these findings, we wanted to explore potential responses of the periodontal tissues to the reduced vasculature. We first assessed levels of hypoxia-inducible factor 1-alpha (HIF-1α) expression. HIF-1α is an inducible transcription factor and the master regulator of cellular responses to hypoxia [32]. Veh treated animals with EP showed a modest increase of HIF-1α expression. Similar findings have been observed in clinical studies, where higher levels of HIF-1α expression were noted in periodontitis compared to gingivitis or patients with healthy gingiva [33]. In ZA or OPG-Fc treated animals with EP, a marked increase in HIF-1α was noted, as early as 1 week after disease initiation and remained at high levels for the duration of the experiment. Interestingly, high levels of HIF-1α are observed in the femoral head of rats during experimentally induced avascular necrosis, suggesting an involvement of the HIF-1α signaling cascade in the pathophysiological process of ischemic osteonecrosis [34].

A direct result of HIF-1α induction is the expression vascular endothelial growth factor (VEGF-A), a growth factor secreted by a variety of cells including PDL fibroblasts [35] and osteoblasts [36]. VEGF-A in return plays a significant role in multiple endothelial cell functions including survival, proliferation, migration and tubulogenesis [37]. VEGF-A levels increased in EP sites compared to healthy, non-EP sites. At 1-week VEGF-A was higher in OPG-Fc and ZA animals, compared to Veh animals. Interestingly, while VEGF-A levels in Veh animals remained relatively stable for the duration of the experiment, they declined in animals on ZA or OPG-Fc, such that they were similar with Veh animals at 2 weeks and significantly attenuated at 4 weeks of treatment. In agreement with our findings at the early time point, induction of both HIF-1α and VEGF expression is noted in cartilage cells in rat and pig models of ischemic femoral head osteonecrosis [34, 38]. The attenuation of VEGF-A induction at later time points in our experiments, despite the high levels of HIF-1α could represent a specific response of the alveolar tissues during ONJ progression and reflect a desensitization of the periodontal tissues to HIF-1α signaling.

VCAM-1 is a cell surface sialoglycoprotein originally identified to be expressed in activated endothelial cells and mediating adhesion of leukocytes during the inflammation process [39]. VCAM-1 is expressed in a variety of human tissues and organs, including dendritic cells, macrophages, cardiac fibroblasts, synoviocytes, as well as in several types of malignant cells and its expression has been associated with pathophysiological conditions such as autoimmune disorders, cardiovascular disease, and infections [39–41]. Because VEGF-A signaling mediates VCAM-1 expression [42, 43], we investigated VCAM-1 levels in periodontal tissues during EP in animals treated with antiresorptives. VCAM-1 was induced in control, ZA or OPG-Fc treated animals during the first two time points, with levels above those seen in healthy, non-EP sites. However, at four weeks, VCAM-1 levels in animals treated with antiresorptives were significantly lower. This decrease in VCAM-1 expression paralleled the attenuation of VEGF-A expression at the same experimental time point, and suggested an altered response of the periodontal tissues in the inflammatory environment of EP during inhibition of bone resorption.

Our results indicated the early onset of altered vascularity and hypoxia, and the subsequent attenuation of signalling cascades associated with neo-angiogenesis and inflammatory response. To examine potential ramifications of the above responses, we then tested the level of oxidative stress in the periodontal tissues, by assessing expression levels of 4 hydroxynonenal (4HNE). 4HNE is a byproduct of lipid peroxidation, with known expression during oxidative stress and implication in oxidative stress induced cell death [44]. We also tested cell apoptosis by evaluating levels of cleaved-caspase-3 expression. Both 4HNE and cleaved-caspase-3 were increased in EP vs. healthy sites. However, high levels of 4HNE and cleaved-caspase-3 expression were noted at all experimental time points in EP sites in animals treated with both antiresorptives. Interestingly, increased oxidative stress levels around areas of established ONJ in patients treated with high-dose BPs have been reported [45, 46]. Our findings are in agreement with these observations and further support that increased oxidative stress is an early event in the process of ONJ pathogenesis. Additionally, ZA treatment of gingival fibroblasts and keratinocyte cell lines is followed by induction of apoptosis and expression of cleaved caspase 3 and 9 [12]. In our studies, both ZA and OPG-Fc treated animals demonstrated increased cleaved caspase 3 expression, suggesting that these changes probably are not only due to a potential direct effect of ZA in the epithelial tissues.

Importantly, throughout our study, changes in marker expression were remarkably similar between animals treated with ZA or OPG-Fc, despite the distinct molecular mechanism of action, pharmacokinetics and clearance of these medications. These observations parallel human and animal studies that report a similar burden of ONJ between bisphosphonates and RANKL inhibitors [9, 21] and indicate that a central parameter in the distinct response of the periodontal tissues during ONJ development is inhibition of osteoclastic differentiation and function.

Our study has certain limitations that need to be considered. The doses of ZA used here exceed the pharmacologic ZA doses used for control of malignancy. We utilized these higher ZA doses in an attempt to ensure efficient development of ONJ lesions in the great majority of the animals. The possibility of an off-target effect of ZA at these supra-pharmacologic doses cannot be excluded. However, the similarity of our findings with two different antiresorptive agents with distinct molecular mechanism of action makes this possibility unlikely. In addition, animals euthanized at early time points were exposed to lower cumulative amounts of ZA or OPG-Fc. However, the expression levels of various biomarkers tested in sites of healthy molars remained similar at all time points. If a toxic effect of the antiresorptives was present, it would be expected that the healthy control sites in each treatment group would demonstrate variable expression with prolonged treatment. Nevertheless, studies evaluating lower and clinically relevant doses should be used to confirm our findings. The use of an anti-angiogenic agent could have provided a positive control on assessing effects in angiogenesis. Finally, the exact nature of cells expressing the various biomarkers and their subcellular localization need further exploration.

In conclusion, our data point to the disruption in the vasculature of the periodontal tissues at sites of EP in antiresorptive-treated animals. These structural changes are accompanied by altered responses to hypoxia, cell adhesion, oxidative stress and ultimately cell apoptosis.

Further experimental exploration is required to characterize how these cellular responses at early stages of disease development evolve to subsequent tissue alterations and ultimately lead to clinical bone exposure, the hallmark presentation of established ONJ.

Supplementary Material

Refer to Web version on PubMed Central for supplementary material.

ACKNOWLEDGEMENTS

This work was supported by grants from NIH/NIDCR R01 DE019465 (ST). DH was supported by T90/R90 DE007296 and F30 DE028171. We gratefully thank Amgen, Inc. for providing OPG-Fc used, and the Translational Pathology Core Laboratory (TPCL) at the David Geffen School of Medicine at UCLA for all histology and digital imaging services.

REFERENCES

[1]. Khan AA, Morrison A, Hanley DA, Felsenberg D, McCauley LK, O'Ryan F, Reid IR, Ruggiero SL, Taguchi A, Tetradis S, Watts NB, Brandi ML, Peters E, Guise T, Eastell R, Cheung AM, Morin SN, Masri B, Cooper C, Morgan SL, Obermayer-Pietsch B, Langdahl BL, Al Dabagh R, Davison KS, Kendler DL, Sandor GK, Josse RG, Bhandari M, El Rabbany M, Pierroz DD, Sulimani R, Saunders DP, Brown JP, Compston J, International J Task Force on Osteonecrosis of the, Diagnosis and management of osteonecrosis of the jaw: a systematic review and international consensus, J Bone Miner Res 30(1) (2015) 3–23. [PubMed: 25414052]

[2]. Ruggiero SL, Dodson TB, Fantasia J, Goodday R, Aghaloo T, Mehrotra B, O'Ryan F, American Association of O, Maxillofacial S, American Association of Oral and Maxillofacial Surgeons position paper on medication-related osteonecrosis of the jaw−-2014 update, J Oral Maxillofac Surg 72(10) (2014) 1938–56. [PubMed: 25234529]

[3]. Marx RE, Sawatari Y, Fortin M, Broumand V, Bisphosphonate-induced exposed bone (osteonecrosis/osteopetrosis) of the jaws: risk factors, recognition, prevention, and treatment, J Oral Maxillofac Surg 63(11) (2005) 1567–75. [PubMed: 16243172]

[4]. Khosla S, Burr D, Cauley J, Dempster DW, Ebeling PR, Felsenberg D, Gagel RF, Gilsanz V, Guise T, Koka S, McCauley LK, McGowan J, McKee MD, Mohla S, Pendrys DG, Raisz LG, Ruggiero SL, Shafer DM, Shum L, Silverman SL, Van Poznak CH, Watts N, Woo SB, Shane E, American Society for B, Mineral R, Bisphosphonate-associated osteonecrosis of the jaw: report of a task force of the American Society for Bone and Mineral Research, J Bone Miner Res 22(10) (2007) 1479–91. [PubMed: 17663640]

[5]. Aghaloo T, Hazboun R, Tetradis S, Pathophysiology of Osteonecrosis of the Jaws, Oral Maxillofac Surg Clin North Am 27(4) (2015) 489–96. [PubMed: 26412796]

[6]. Allen MR, Medication-Related Osteonecrosis of the Jaw: Basic and Translational Science Updates, Oral Maxillofac Surg Clin North Am 27(4) (2015) 497–508. [PubMed: 26277349]

[7]. Ruggiero SL, Dodson TB, Assael LA, Landesberg R, Marx RE, Mehrotra B, O. American Association of, S. Maxillofacial, American Association of Oral and Maxillofacial Surgeons position paper on bisphosphonate-related osteonecrosis of the jaws−-2009 update, J Oral Maxillofac Surg 67(5 Suppl) (2009) 2–12.

[8]. Reid IR, Bolland MJ, Grey AB, Is bisphosphonate-associated osteonecrosis of the jaw caused by soft tissue toxicity?, Bone 41(3) (2007) 318–20. [PubMed: 17572168]

[9]. Soundia A, Hadaya D, Esfandi N, de Molon RS, Bezouglaia O, Dry SM, Pirih FQ, Aghaloo T, Tetradis S, Osteonecrosis of the jaws (ONJ) in mice after extraction of teeth with periradicular disease, Bone 90 (2016) 133–41. [PubMed: 27327410]

[10]. Donetti E, Gualerzi A, Sardella A, Lodi G, Carrassi A, Sforza C, Alendronate impairs epithelial adhesion, differentiation and proliferation in human oral mucosa, Oral Dis 20(5) (2014) 466–72. [PubMed: 23837876]

[11]. Agis H, Beirer B, Watzek G, Gruber R, Effects of carboxymethylcellulose and hydroxypropylmethylcellulose on the differentiation and activity of osteoclasts and osteoblasts, J Biomed Mater Res A 95(2) (2010) 504–9. [PubMed: 20665677]

[12]. Scheper MA, Badros A, Chaisuparat R, Cullen KJ, Meiller TF, Effect of zoledronic acid on oral fibroblasts and epithelial cells: a potential mechanism of bisphosphonate-associated osteonecrosis, Br J Haematol 144(5) (2009) 667–76. [PubMed: 19036117]

[13]. Mozzati M, Martinasso G, Maggiora M, Scoletta M, Zambelli M, Carossa S, Oraldi M, Muzio G, Canuto RA, Oral mucosa produces cytokines and factors influencing osteoclast activity and endothelial cell proliferation, in patients with osteonecrosis of jaw after treatment with zoledronic acid, Clin Oral Investig 17(4) (2013) 1259–66.

[14]. Ishtiaq S, Edwards S, Sankaralingam A, Evans BA, Elford C, Frost ML, Fogelman I, Hampson G, The effect of nitrogen containing bisphosphonates, zoledronate and alendronate, on the production of pro-angiogenic factors by osteoblastic cells, Cytokine 71(2) (2015) 154–60. [PubMed: 25461393]

[15]. Bi Y, Gao Y, Ehirchiou D, Cao C, Kikuiri T, Le A, Shi S, Zhang L, Bisphosphonates cause osteonecrosis of the jaw-like disease in mice, Am J Pathol 177(1) (2010) 280–90. [PubMed: 20472893]

[16]. Bastos P, Patel V, Festy F, Hosny N, Cook RJ, In-vivo imaging of the microvasculature of the soft tissue margins of osteonecrotic jaw lesions, Br Dent J 223(9) (2017) 699–705. [PubMed: 29123273]

[17]. Aghaloo TL, Kang B, Sung EC, Shoff M, Ronconi M, Gotcher JE, Bezouglaia O, Dry SM, Tetradis S, Periodontal disease and bisphosphonates induce osteonecrosis of the jaws in the rat, J Bone Miner Res 26(8) (2011) 1871–82. [PubMed: 21351151]

[18]. Kang B, Cheong S, Chaichanasakul T, Bezouglaia O, Atti E, Dry SM, Pirih FQ, Aghaloo TL, Tetradis S, Periapical disease and bisphosphonates induce osteonecrosis of the jaws in mice, J Bone Miner Res 28(7) (2013) 1631–40. [PubMed: 23426919]

[19]. Ominsky MS, Li X, Asuncion FJ, Barrero M, Warmington KS, Dwyer D, Stolina M, Geng Z, Grisanti M, Tan HL, Corbin T, McCabe J, Simonet WS, Ke HZ, Kostenuik PJ, RANKL inhibition with osteoprotegerin increases bone strength by improving cortical and trabecular bone architecture in ovariectomized rats, J Bone Miner Res 23(5) (2008) 672–82. [PubMed: 18433301]

[20]. de Molon RS, Hsu C, Bezouglaia O, Dry SM, Pirih FQ, Soundia A, Cunha FQ, Cirelli JA, Aghaloo TL, Tetradis S, Rheumatoid Arthritis Exacerbates the Severity of Osteonecrosis of the Jaws (ONJ) in Mice. A Randomized, Prospective, Controlled Animal Study, J Bone Miner Res 31(8) (2016) 1596–607. [PubMed: 26950411]

[21]. de Molon RS, Shimamoto H, Bezouglaia O, Pirih FQ, Dry SM, Kostenuik P, Boyce RW, Dwyer D, Aghaloo TL, Tetradis S, OPG-Fc but Not Zoledronic Acid Discontinuation Reverses Osteonecrosis of the Jaws (ONJ) in Mice, J Bone Miner Res 30(9) (2015) 1627–40. [PubMed: 25727550]

[22]. Fondi C, Franchi A, Definition of bone necrosis by the pathologist, Clin Cases Miner Bone Metab 4(1) (2007) 21–6. [PubMed: 22460748]

[23]. Guo DC, Papke CL, Tran-Fadulu V, Regalado ES, Avidan N, Johnson RJ, Kim DH, Pannu H, Willing MC, Sparks E, Pyeritz RE, Singh MN, Dalman RL, Grotta JC, Marian AJ, Boerwinkle EA, Frazier LQ, LeMaire SA, Coselli JS, Estrera AL, Safi HJ, Veeraraghavan S, Muzny DM, Wheeler DA, Willerson JT, Yu RK, Shete SS, Scherer SE, Raman CS, Buja LM, Milewicz DM, Mutations in smooth muscle alpha-actin (ACTA2) cause coronary artery disease, stroke, and Moyamoya disease, along with thoracic aortic disease, Am J Hum Genet 84(5) (2009) 617–27. [PubMed: 19409525]

[24]. dela Paz NG, D'Amore PA, Arterial versus venous endothelial cells, Cell Tissue Res 335(1) (2009) 5–16. [PubMed: 18972135]

[25]. Aguiar Bujanda D, Bohn Sarmiento U, Cabrera Suarez MA, Aguiar Morales J, Assessment of renal toxicity and osteonecrosis of the jaws in patients receiving zoledronic acid for bone metastasis, Ann Oncol 18(3) (2007) 556–60. [PubMed: 17082512]

[26]. Jadu F, Lee L, Pharoah M, Reece D, Wang L, A retrospective study assessing the incidence, risk factors and comorbidities of pamidronate-related necrosis of the jaws in multiple myeloma patients, Ann Oncol 18(12) (2007) 2015–9. [PubMed: 17804475]

[27]. Hadaya D, Soundia A, Freymiller E, Grogan T, Elashoff D, Tetradis S, Aghaloo TL, Nonsurgical Management of Medication-Related Osteonecrosis of the Jaws Using Local Wound Care, J Oral Maxillofac Surg (2018).

[28]. Soundia A, Hadaya D, Esfandi N, Gkouveris I, Christensen R, Dry SM, Bezouglaia O, Pirih F, Nikitakis N, Aghaloo T, Tetradis S, Zoledronate Impairs Socket Healing after Extraction of Teeth with Experimental Periodontitis, J Dent Res 97(3) (2018) 312–320. [PubMed: 28954199]

[29]. Zhang Q, Atsuta I, Liu S, Chen C, Shi S, Shi S, Le AD, IL-17-mediated M1/M2 macrophage alteration contributes to pathogenesis of bisphosphonate-related osteonecrosis of the jaws, Clin Cancer Res 19(12) (2013) 3176–88. [PubMed: 23616636]

[30]. Hadaya D, Soundia A, Gkouveris I, Dry SM, Aghaloo TL, Tetradis S, Development of Medication-Related Osteonecrosis of the Jaw After Extraction of Teeth With Experimental Periapical Disease, J Oral Maxillofac Surg (2018).

[31]. Aguirre JI, Akhter MP, Kimmel DB, Pingel JE, Williams A, Jorgensen M, Kesavalu L, Wronski TJ, Oncologic doses of zoledronic acid induce osteonecrosis of the jaw-like lesions in rice rats (Oryzomys palustris) with periodontitis, J Bone Miner Res 27(10) (2012) 2130–43. [PubMed: 22623376]

[32]. Iyer NV, Kotch LE, Agani F, Leung SW, Laughner E, Wenger RH, Gassmann M, Gearhart JD, Lawler AM, Yu AY, Semenza GL, Cellular and developmental control of O2 homeostasis by hypoxia-inducible factor 1 alpha, Genes Dev 12(2) (1998) 149–62. [PubMed: 9436976]

[33]. Vasconcelos RC, Costa Ade L, Freitas Rde A, Bezerra BA, Santos BR, Pinto LP, Gurgel BC, Immunoexpression of HIF-1αlpha and VEGF in Periodontal Disease and Healthy Gingival Tissues, Braz Dent J 27(2) (2016) 117–22. [PubMed: 27058371]

[34]. Zhang W, Yuan Z, Pei X, Ma R, In vivo and in vitro characteristic of HIF-1αlpha and relative genes in ischemic femoral head necrosis, Int J Clin Exp Pathol 8(6) (2015) 7210–6. [PubMed: 26261616]

[35]. Yanagita M, Kojima Y, Kubota M, Mori K, Yamashita M, Yamada S, Kitamura M, Murakami S, Cooperative effects of FGF-2 and VEGF-A in periodontal ligament cells, J Dent Res 93(1)(2014) 89–95. [PubMed: 24186558]

[36]. Hu K, Olsen BR, Osteoblast-derived VEGF regulates osteoblast differentiation and bone formation during bone repair, J Clin Invest 126(2) (2016) 509–26. [PubMed: 26731472]

[37]. Zachary I, VEGF signalling: integration and multi-tasking in endothelial cell biology, Biochem Soc Trans 31(Pt 6) (2003) 1171–7. [PubMed: 14641020]

[38]. Zhang C, Li Y, Cornelia R, Swisher S, Kim H, Regulation of VEGF expression by HIF 1alpha in the femoral head cartilage following ischemia osteonecrosis, Sci Rep 2 (2012) 650. [PubMed: 22970342]

[39]. Schlesinger M, Bendas G, Vascular cell adhesion molecule-1 (VCAM-1)--an increasing insight into its role in tumorigenicity and metastasis, Int J Cancer 136(11) (2015) 2504–14. [PubMed: 24771582]

[40]. Olivares-Silva F, Landaeta R, Aranguiz P, Bolivar S, Humeres C, Anfossi R, Vivar R, Boza P, Munoz C, Pardo-Jimenez V, Peiro C, Sanchez-Ferrer CF, Diaz-Araya G, Heparan sulfate potentiates leukocyte adhesion on cardiac fibroblast by enhancing Vcam-1 and Icam-1 expression, Biochim Biophys Acta 1864(3) (2017) 831–842.

[41]. Li P, Sanz I, O'Keefe RJ, Schwarz EM, NF-kappa B regulates VCAM-1 expression on fibroblast-like synoviocytes, J Immunol 164(11) (2000) 5990–7. [PubMed: 10820282]

[42]. Ramakrishnan S, Anand V, Roy S, Vascular endothelial growth factor signaling in hypoxia and inflammation, J Neuroimmune Pharmacol 9(2) (2014) 142–60. [PubMed: 24610033]

[43]. Kim I, Moon SO, Kim SH, Kim HJ, Koh YS, Koh GY, Vascular endothelial growth factor expression of intercellular adhesion molecule 1 (ICAM-1), vascular cell adhesion molecule 1 (VCAM-1), and E-selectin through nuclear factor-kappa B activation in endothelial cells, J Biol Chem 276(10) (2001) 7614–20. [PubMed: 11108718]

[44]. Ayala A, Munoz MF, Arguelles S, Lipid peroxidation: production, metabolism, and signaling mechanisms of malondialdehyde and 4-hydroxy-2-nonenal, Oxid Med Cell Longev 2014 (2014)360438. [PubMed: 24999379]

[45]. Bagan J, Saez GT, Tormos MC, Gavalda-Esteve C, Bagan L, Leopoldo-Rodado M, Calvo J, Camps C, Oxidative stress in bisphosphonate-related osteonecrosis of the jaws, J Oral Pathol Med 43(5) (2014) 371–7. [PubMed: 24450511]

[46]. Kocer M, Naziroglu M, Kocer G, Sonmez TT, Effects of bisphosphonate on oxidative stress levels in patients with different types of cancer, Cancer Invest 32(2) (2014) 37–42. [PubMed: 24308847]

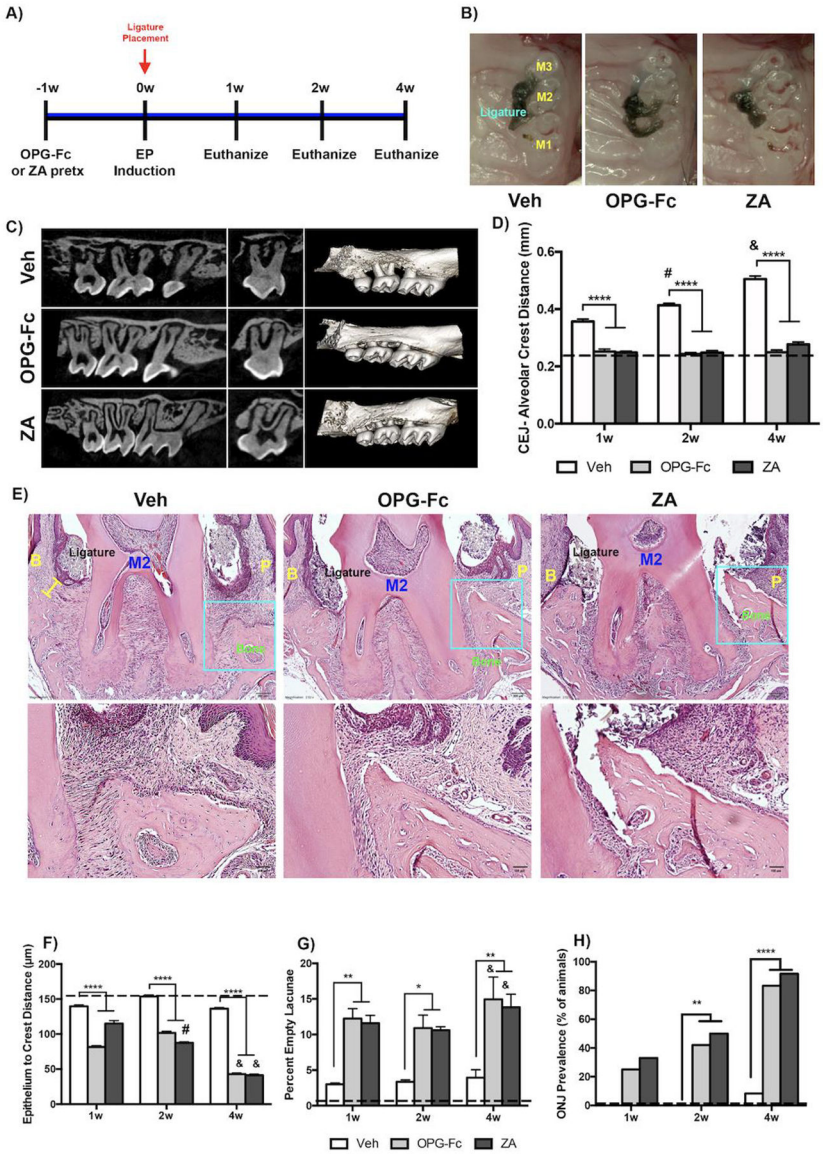

Figure 1: Radiographic and Histologic Measurement of Veh, OPG-Fc, and ZA treated animals.

A) Experimental Timeline. B) Clinical photomicrographs of Veh, OPG-Fc or ZA treated animals. C) Parasagittal and coronal cross sections and 3-dimensional μCT reconstructions of Veh, OPGFc or ZA animals at the 4-week time point D) Quantification of the CEJ-Alveolar Crest Distance for Veh, OPG-Fc, and ZA treated animals, at the 1-week, 2-week, and 4-week time points. E) Representative coronal H&E images of Veh, OPG-Fc, and ZA treated animals at the 4 weeks after ligature placement. F) Quantification of the epithelium to crest distance. G) Quantification of the percent empty osteocytic lacunae. H) ONJ Prevalence at the 4-week time point. The yellow bar denotes the Epithelium to Alveolar Crest Distance. Data represents mean value ± SEM. **** = statistical significance $p<0.0001$, *** = statistical significance $p<0.001$, ** = statistical significance $p<0.01$, * = statistical significance $p<0.05$. *% statistical significance $p<0.05$ vs 1w. & = statistical significance

p<0.05 vs 1w and 2w. # = statistical significant vs. 1w. M1= First Molar, M2= Second Molar, M3= Third Molar. B= Buccal; P=Palatal.

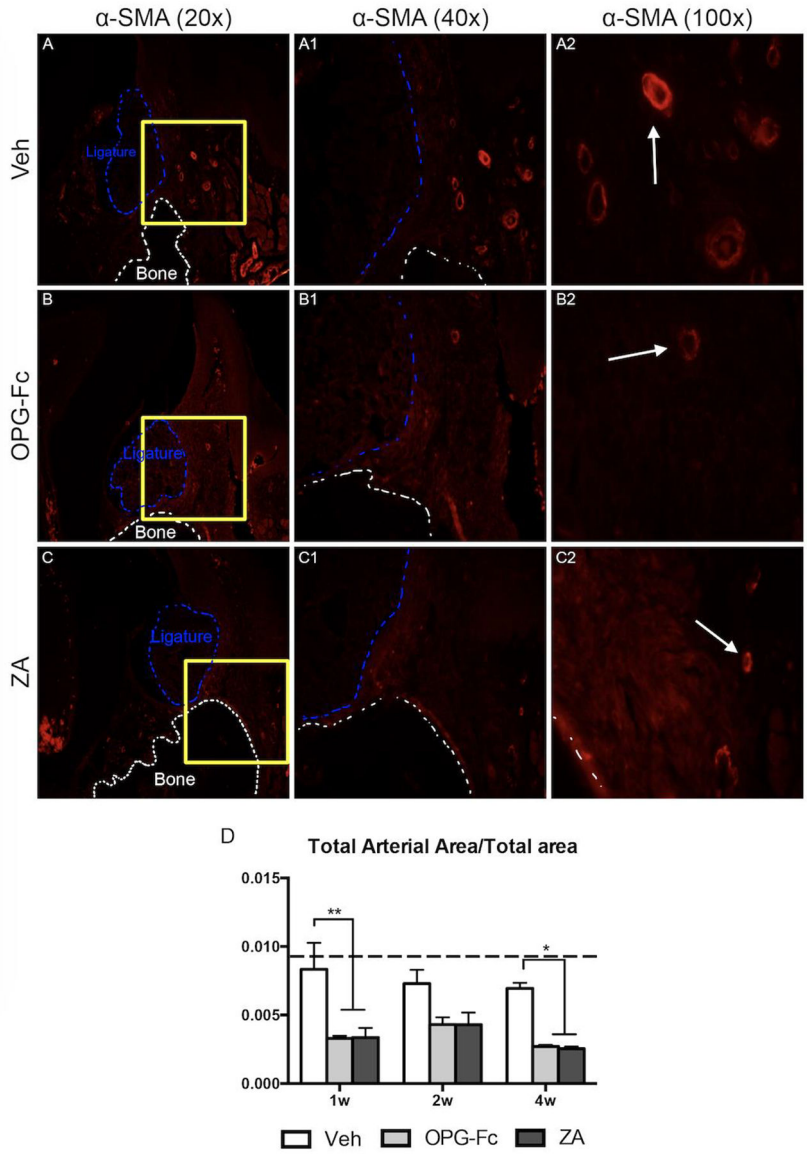

Figure 2: Alpha-Smooth Muscle Actin Immunofluorescence Staining of Veh, OPG-Fc, and ZA treated animals 1 week following Ligature Placement.

A-A2) 20x, 40x, and 100x magnification of alpha-SMA immunofluorescence staining of Veh treated animals. B-B2) 20x, 40x, and 100x magnification of alpha-SMA immunofluorescence staining of OPG-Fc treated animals. C-C2) 20x, 40x, and 100x magnification of alpha-SMA immunofluorescence staining of ZA treated animals. D) Quantification of the Total Arterial Area/Total area. The white dotted lines outline the bone and the blue dotted line outlines the ligature. Data represents mean value ± SEM. **** = statistical significance $p<0.0001$, *** = statistical significance $p<0.001$, ** = statistical significance $p<0.01$, * = statistical significance $p<0.05$.

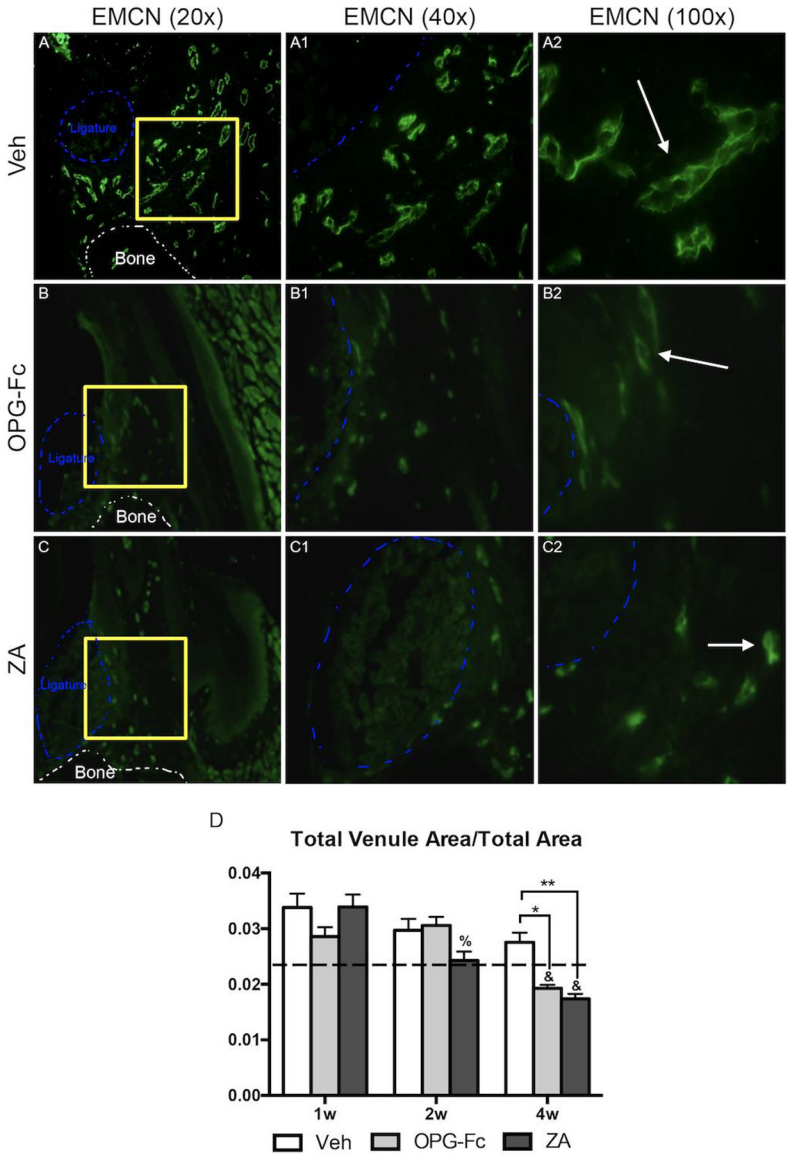

Figure 3: Endomucin Immunofluorescence Staining of Veh, OPG-Fc, and ZA treated animals 4 weeks following Ligature Placement.

A-A2) 20x, 40x, and 100x magnification of EMCN immunofluorescence staining of Veh treated animals. B-B2) 20x, 40x, and 100x magnification of EMCN immunofluorescence staining of OPG-Fc treated animals. C-C2) 20x, 40x, and 100x magnification of EMCN immunofluorescence staining of ZA treated animals. D) Quantification of the Total Venule Area/Total area. The white dotted lines outline the bone and the blue dotted line outlines the ligature. Data represents mean value ± SEM. **** = statistical significance $p<0.0001$, *** = statistical significance $p<0.001$, ** = statistical significance $p<0.01$, * = statistical significance $p<0.05$. % statistical significance $p<0.05$ vs 1w. & = statistical significance $p<0.05$ vs 1w and 2w. # = statistical significant vs. 1w.

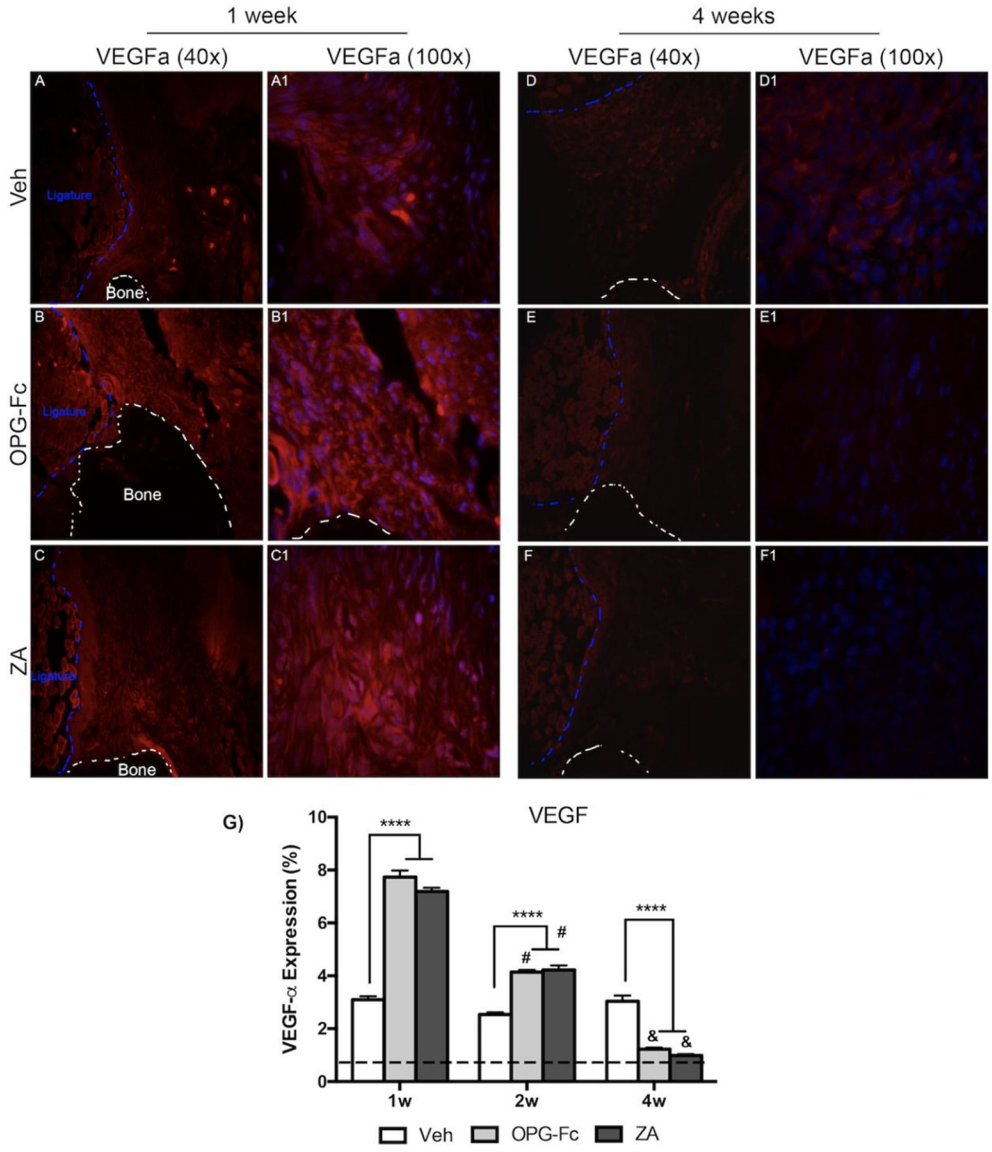

Figure 4: VEGF Immunofluorescence Staining of Veh, OPG-Fc, and ZA treated animals 1 and 4 weeks following Ligature Placement.

A-A1) 40x and 100x magnification of VEGF immunofluorescence staining of Veh treated animals 1 following ligature placement. B-B1) 40x and 100x magnification of VEGF immunofluorescence staining of OPG-Fc treated animals at the 1 week timepoint. C-C1) 40x and 100x magnification of VEGF immunofluorescence staining of ZA treated animals after 1 week of experimental periodontitis. D-D1) 40x and 100x magnification of VEGF immunofluorescence staining of Veh treated animals 4 weeks after ligature placement. E-E1) 40x and 100x magnification of VEGF immunofluorescence staining of OPG-Fc treated animals at the 4 week timepoint. F-F1) 40x and 100x magnification of VEGF immunofluorescence staining of ZA treated animals after 4 weeks of experimental periodontitis. G) Quantification of the VEGF expression. The dotted line represents expression in the healthy periodontium. The white dotted lines outline the bone and the blue dotted line outlines the ligature. Data represents mean value ± SEM. **** = statistical

significance p<0.0001, *** = statistical significance p<0.001, ** = statistical significance p<0.01, * = statistical significance p<0.05. *%* statistical significance p<0.05 vs 1w. & = statistical significance p<0.05 vs 1w and 2w. # = statistical significant vs. 1w.

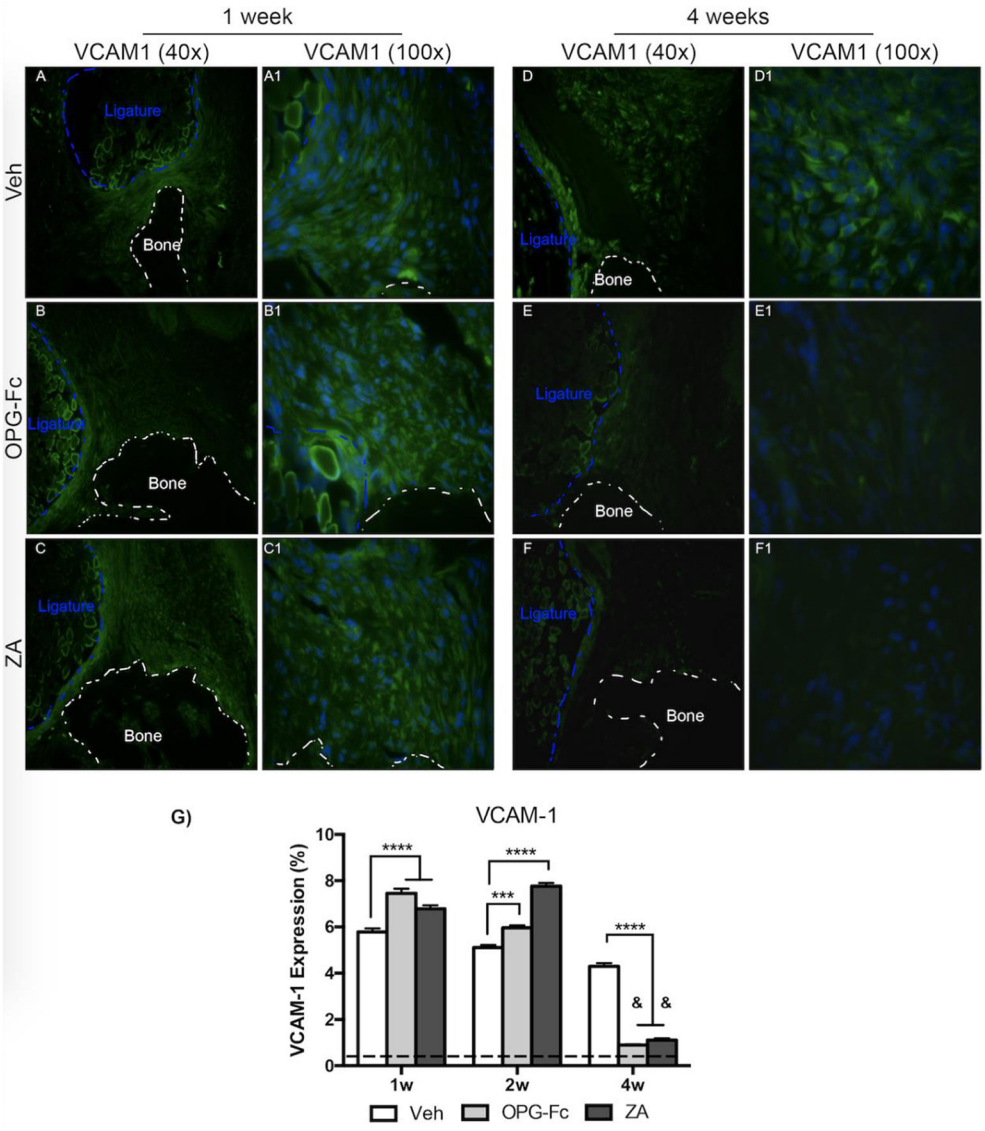

Figure 5: VCAM-1 Immunofluorescence Staining of Veh, OPG-Fc, and ZA treated animals 1 and 4 weeks following Ligature Placement.

A-A1) 40x and 100x magnification of VCAM-1 immunofluorescence staining of Veh treated animals 1 week following ligature placement. B-B1) 40x and 100x magnification of VCAM-1 immunofluorescence staining of OPG-Fc treated animals 1 week following experimental periodontitis. C-C1) 40x and 100x magnification of VCAM-1 immunofluorescence staining of ZA treated animals at the 1-week time-point. D-D1) 40x and 100x magnification of VCAM-1 immunofluorescence staining of Veh treated animals 4 weeks after ligature placement. E-E1) 40x and 100x magnification of VCAM-1 immunofluorescence staining of OPG-Fc treated animals 4 weeks following experimental periodontitis. F-F1) 40x and 100x magnification of VCAM-1 immunofluorescence staining of ZA treated animals at the 4-week time-point. G) Quantification of the VCAM-1 expression. The dotted line represents expression in the healthy periodontium. The white dotted lines outline the bone and the blue dotted line outlines the ligature. Data represents

mean value ± SEM. **** = statistical significance $p<0.0001$, *** = statistical significance $p<0.001$, ** = statistical significance $p<0.01$, * = statistical significance $p<0.05$. % statistical significance $p<0.05$ vs 1w. & = statistical significance $p<0.05$ vs 1w and 2w. # = statistical significant vs. 1w.

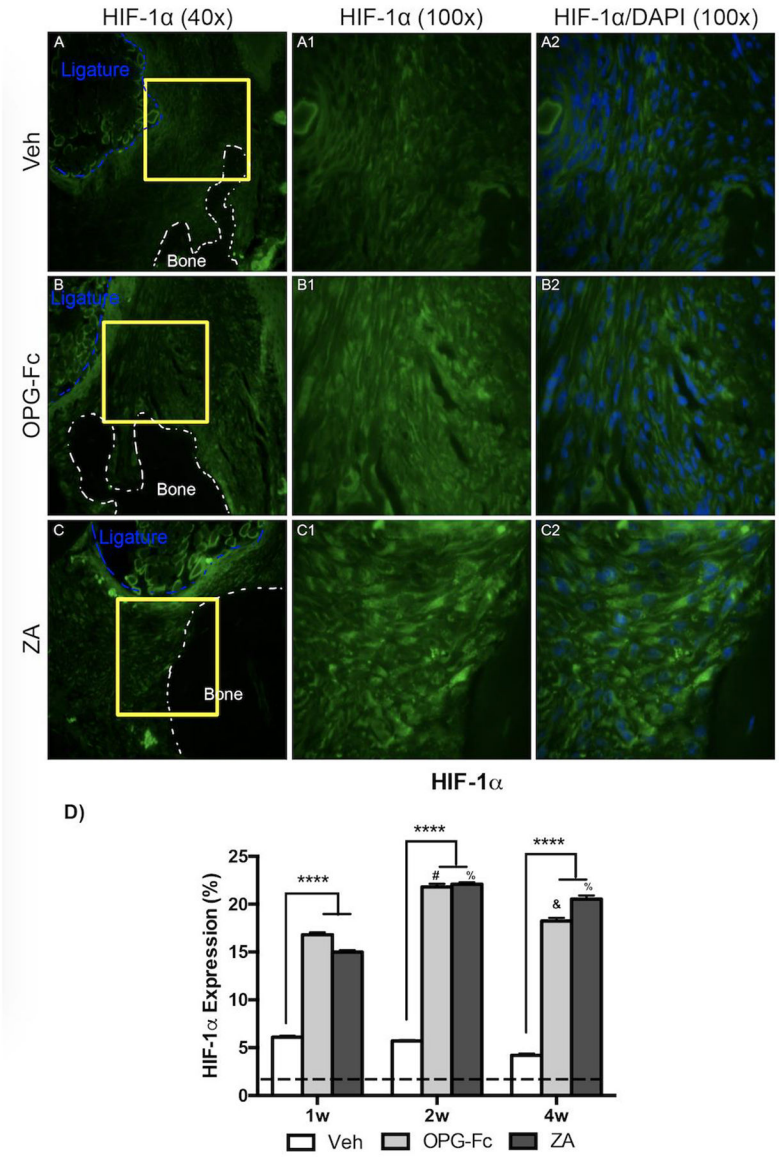

Figure 6: HIF-1a Immunofluorescence Staining of Veh, OPG-Fc, and ZA treated animals 2 weeks following Ligature Placement.

A-A1) 40x and 100x magnification of HIF-1a staining in Veh treated animals. A2) HIF-1a and DAPI immunofluorescence stains merged at 100x magnification of Veh treated animals. B-B1) 40x and 100x magnification of HIF-1a staining in OPG-Fc treated animals. B2) HIF-1a and DAPI immunofluorescence stains merged at 100x magnification of OPG-Fc treated animals. C-C1) 40x and 100x magnification of HIF-1a staining in ZA treated animals. C2) HIF-1a and DAPI immunofluorescence stains merged at 100x magnification of ZA treated animals. D) Quantification of the HIF-1a expression at all 3 time points. The dotted line represents expression in the healthy periodontium. The white dotted lines outline the bone and the blue dotted line outlines the ligature. Data represents mean value ± SEM. **** = statistical significance p<0.0001, *** = statistical significance p<0.001, ** = statistical significance p<0.01, * = statistical significance p<0.05. *%* statistical significance

$p<0.05$ vs 1w. & = statistical significance $p<0.05$ vs 1w and 2w. # = statistical significant vs. 1w.

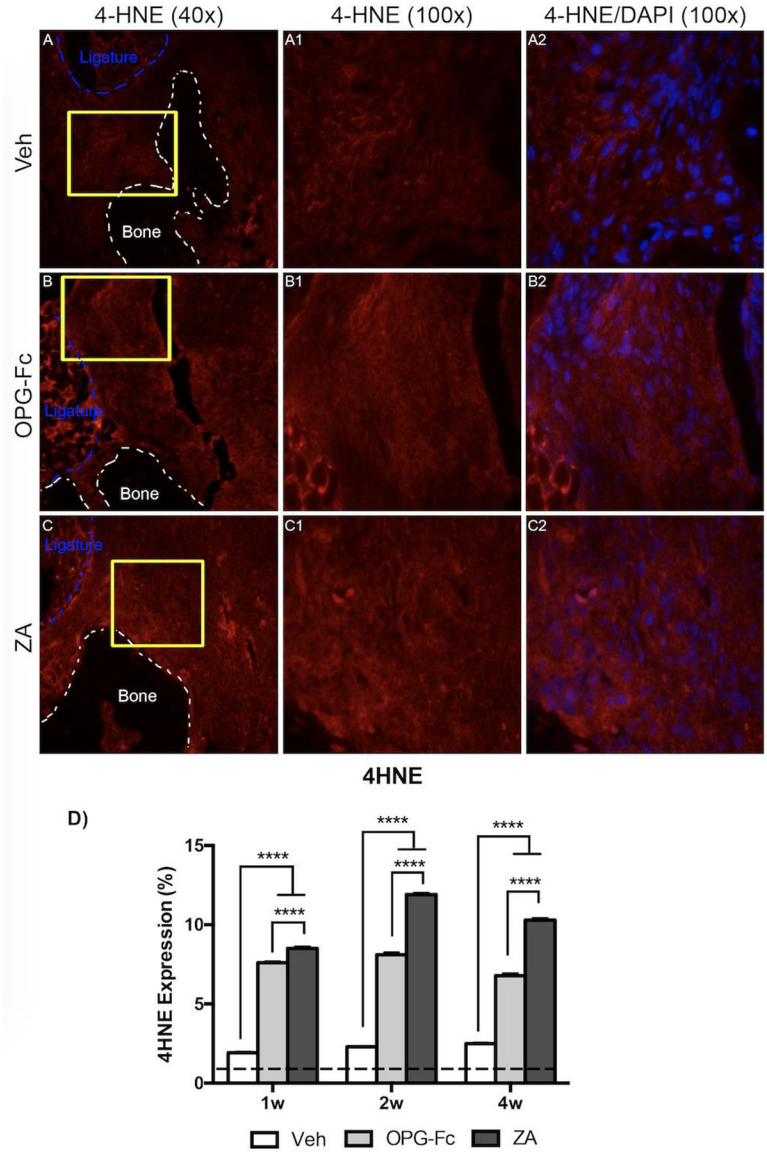

Figure 7: 4HNE Immunofluorescence Staining of Veh, OPG-Fc, and ZA treated animals 1 week following Ligature Placement.

A-A1) 40x and 100x magnification of 4HNE staining in Veh treated animals. A2) 4HNE and DAPI immunofluorescence stains merged at 100x magnification of Veh treated animals. B-B1) 40x and 100x magnification of 4HNE staining in OPG-Fc treated animals. B2) 4HNE and DAPI immunofluorescence stains merged at 100x magnification of OPG-Fc treated animals. C-C1) 40x and 100x magnification of 4HNE staining in ZA treated animals. C2) 4HNE and DAPI immunofluorescence stains merged at 100x magnification of ZA treated animals. D) Quantification of the 4HNE expression at all 3 time points. The dotted line represents expression in the healthy periodontium. The white dotted lines outline the bone and the blue dotted line outlines the ligature. Data represents mean value ± SEM. **** = statistical significance $p<0.0001$, *** = statistical significance $p<0.001$, ** = statistical significance $p<0.01$, * = statistical significance $p<0.05$. % statistical significance $p<0.05$ vs 1w. & = statistical significance $p<0.05$ vs 1w and 2w. # = statistical significant vs. 1w.

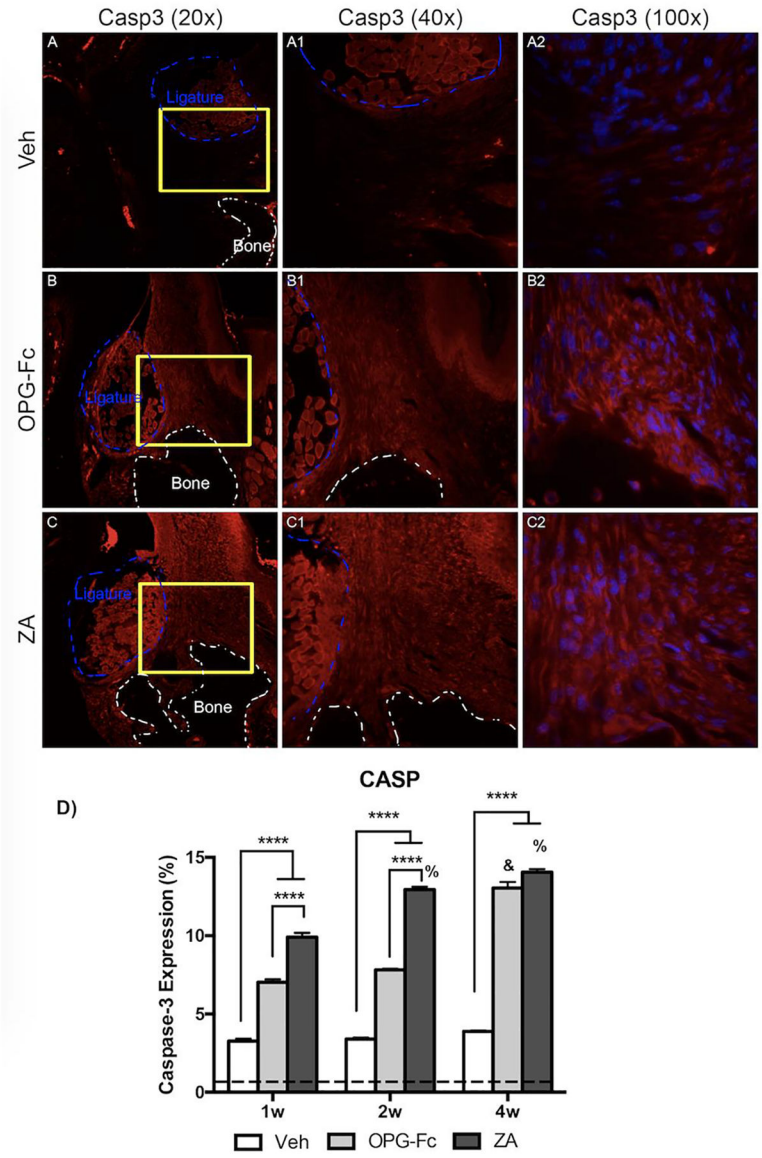

Figure 8: Caspase-3 Immunofluorescence Staining of Veh, OPG-Fc, and ZA treated animals 4 weeks following Ligature Placement.

A-A2) 20x, 40x, and 100x magnification, respectively, of caspase-3 immunofluorescence staining of Veh treated animals. B-B2) 20x, 40x, and 100x magnification, respectively, of caspase-3 immunofluorescence staining of OPG-Fc treated animals. C-C2) 20x, 40x, and 100x magnification, respectively, of caspase-3 immunofluorescence staining of ZA treated animals. D) Quantification of the caspase-3 expression at all 3 time points. The dotted line represents expression in the healthy periodontium. The white dotted lines outline the bone and the blue dotted line outlines the ligature. Data represents mean value ± SEM. **** = statistical significance $p<0.0001$, *** = statistical significance $p<0.001$, ** = statistical significance $p<0.01$, * = statistical significance $p<0.05$. % statistical significance $p<0.05$ vs 1w. & = statistical significance $p<0.05$ vs 1w and 2w. # = statistical significant vs. 1w.